Experiments on the $2\,^3P$ state of helium. III. Measurement of the $2\,^3P_0$-$2\,^3P_1$ fine-structure interval

A. Kponou, V. W. Hughes, C. E. Johnson,* S. A. Lewis,† and F. M. J. Pichanick‡
Gibbs Laboratory, Physics Department, Yale University, New Haven, Connecticut 06520
(Received 4 August 1980)

The $2\,^3P_0$-$2\,^3P_1$ fine-structure interval ν_{01} has been measured using the optical-microwave atomic beam magnetic resonance technique. The result, a major improvement upon previous measurements, is $\nu_{01} = 29\,616.864 \pm 0.036$ MHz (1.2 ppm). This compares well with the latest theoretical value $\nu_{01} = 29\,616.914 \pm 0.043$ MHz (1.4 ppm), and provides an important test of the theory of fine structure of the two-electron atom. Alternatively, our experiment can be regarded as an independent measurement of the fine-structure constant with the result $\alpha^{-1} = 137.036\,08 \pm 0.000\,13$ (0.94 ppm), which is consistent with the more accurate currently accepted value $\alpha^{-1} = 137.035\,963 \pm 0.000\,015$ (0.11 ppm).

I. INTRODUCTION

Earlier papers[1] (referred to hereafter as I and II) describing measurements of the $2\,^3P_1$-$2\,^3P_2$ fine-structure interval of helium and of the Zeeman effect in the $2\,^3P$ state have discussed at some length the motivation for these experiments. Measurement of the fine structure of the triplet states of helium can provide a very accurate check of the application of quantum electrodynamics to the two-electron bound-state problem, and it also offers the possibility of determining the value of the fine-structure constant α to a very high accuracy. The presently accepted value of α was determined mainly from measurements of $2e/h$ utilizing the *ac* Josephson effect, in conjunction with a recent measurement of the proton gyromagnetic ratio.[2] Recent determinations of α from muonium hyperfine structure[3] and from the electron $(g\text{-}2)$ value[4] are in good agreement with this accepted value.

Experimentally, the fine structure of helium in the $2\,^3P$ state can and now has been measured to very high precision. The favorable conditions for this measurement are (i) the relatively long lifetime of the $2\,^3P$ state, 1.0×10^{-7} sec, as compared to 1.6×10^{-9} sec for the $2\,^2P$ state of hydrogen, and (ii) the size of the intervals are of the same order of magnitude as the $2\,^2P_{3/2}$-$2\,^2P_{1/2}$ splitting in hydrogen. Taken together, these conditions give for the $2\,^3P_0$-$2\,^3P_1$ and $2\,^3P_1$-$2\,^3P_2$ intervals, respectively, a ratio of fine-structure interval to natural linewidth of about 85 and 7 times greater than the similar ratio for hydrogen. Unlike the hydrogen fine-structure experiments, the helium fine-structure measurements are quite insensitive to electric fields because of the very large $2\,^3S$-$2\,^3P$ separation.

The magnitudes of the fine-structure intervals ν_{12} and ν_{01} of the $2\,^3P$ state are about 2.3 and 30 GHz, respectively. The smaller interval has been measured by two kinds of microwave spectroscopic technique[1,5] and by the level-crossing technique.[6] The larger interval also has been measured by the latter technique. The present paper describes the first microwave spectroscopic measurement of the larger interval, and is by far more accurate. Recent developments in the theoretical calculations[7] will be summarized and discussed in Sec. VII.

The approach used in making the measurement has been described in I. The energy-level scheme for helium is shown in Fig. 1. Metastable $2\,^3S_1$

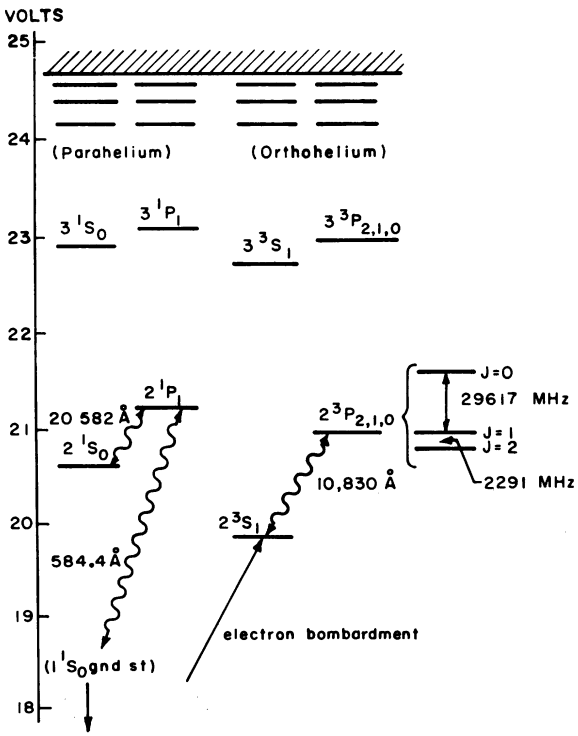

FIG. 1. Lowest excited states of helium. The $2\,^3P$ fine structure is magnified. Radiative processes important in our experiment are indicated by the wavy arrows. The $2\,^3S$ state is produced by electron bombardment.

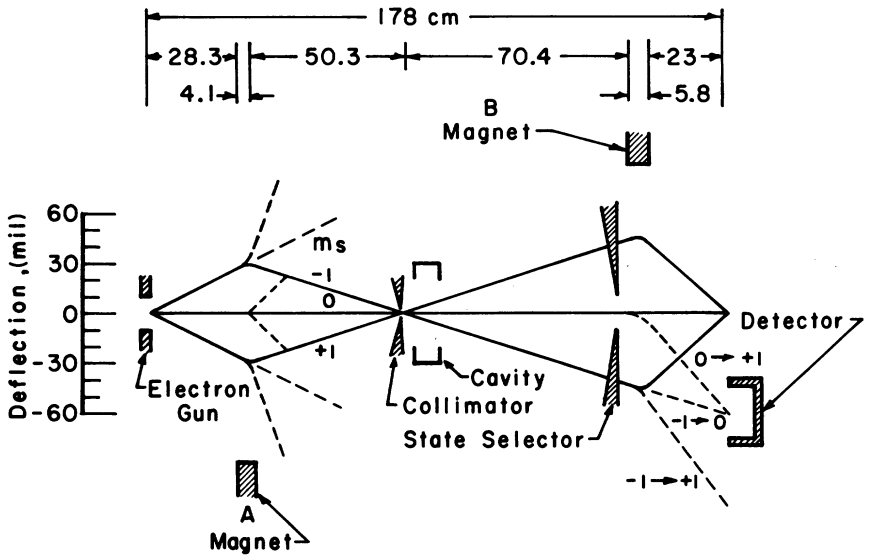

FIG. 2. 2^3S beam atom trajectories. Atoms with improper m_S values at A magnet are deflected out of the beam. Dashed lines after B magnet are trajectories of atoms whose m_S value changes due to $2\,^3S \leftrightarrow 2\,^3P$ transitions in the cavity. The detector is arranged for $2\,^3S$, $0 \rightarrow +1$ signals.

atoms are produced by electron bombardment of $1\,^1S_1$ ground-state atoms in an electron gun. The trajectories of the $2\,^3S_1$ beam are shown in Fig. 2. After passing through the B magnet, the $m_S = 0$ beam reaches the detector. In the C magnet region resonance radiation from a helium discharge lamp excites metastable $m_S = 0$ atoms to the $2\,^3P$ levels. The $2\,^3P$ state atoms decay spontaneously back to the $2\,^3S_1$ sublevels with a mean lifetime of 1.0×10^{-7} sec, and some of the decaying atoms end up in final substates $m_S = \pm1$. At the B magnet these atoms are deflected out of the $m_S = 0$ beam and may be measured by a detector at the appropriate location. A microwave magnetic resonance between $2\,^3P$ sublevels can be observable if it results in a further change in the population of the $m_S = \pm1$ sublevels after radiative decay.

Section II treats the energy levels arising from the fine structure and Zeeman effect and also illustrates the calculations of the signal strength. The choice of transition is also discussed. The apparatus is described in Sec. III. A study of the performance of the apparatus is reported in Sec. IV as part of the experimental procedure. Section V treats the data analysis, possible systematic effects are summarized in Sec. VI, and results are discussed in Sec. VII.

II. THEORY OF THE EXPERIMENT

A. Energy levels

The energy levels of the $2\,^3P$ state associated with the fine structure and Zeeman effect have been discussed in papers I and II. The relevant Hamiltonian is written in the form

$$\vec{\mathcal{H}} = \vec{\mathcal{H}}_{fs} + g_S' \mu_B \vec{S}\cdot\vec{H} + g_L' \mu_B \vec{L}\cdot\vec{H}$$

$$= \vec{\mathcal{H}}_{fs} + g_S' \mu_B S_z H + g_L' \mu_B L_z H\,. \qquad (1)$$

The operator $\vec{\mathcal{H}}_{fs}$ contains the spin-orbit and spin-spin terms which result in the fine structure.[7] The remaining terms are the Zeeman operators due to the uniform field $\vec{H}$ in the z direction. $\vec{L}$ and $\vec{S}$ are, respectively, the total orbital and spin angular momentum operators, and μ_B is the Bohr magneton. The factors $g_S' = 2.002\,243 \pm 0.000\,002$ and $g_L' = 0.999\,867 \pm 0.000\,009$ were determined in

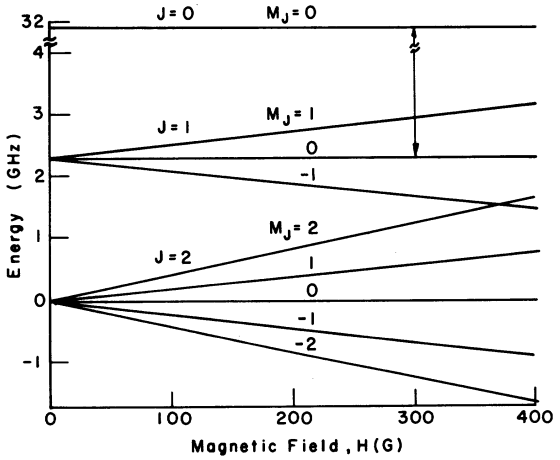

FIG. 3. Zeeman energy-level diagram of the $2\,^3P$ state of helium. The microwave transition, number 15 (Ref. 8), is indicated at a typical value of the magnetic field at which it was observed.

II to sufficient accuracy for our purpose.

The operator $\mathcal{H}_{fs}$ is diagonal in $\vec{J}$ $(=\vec{L}+\vec{S})$ and our experiment determines differences between its eigenvalues E_J. The Zeeman operators couple terms of different J which have the same m_J. We have set up the Hamiltonian in a representation with the angular momentum eigenfunctions $\Psi(J, m_J)$ as bases. The matrix representation of $\mathcal{H}$ is a set of submatrices, one for each value of m_J, which were summarized in paper I. The eigenvalues of these submatrices give the energy levels which are illustrated in Fig. 3 as a function of H, and further details are in Appendix A of I. In the present work we observed a magnetic dipole transition ($J=0$, $m_J=0 \leftrightarrow J=1$, $m_J=0$).[8] The transition frequency is independent of H to first order, and to second order it may be written

$$\nu=(E_0-E_1)+\frac{[(g_S'-g_L')\mu_B H]^2}{3}\left(\frac{4}{E_0-E_1}-\frac{1}{E_1-E_2}\right), \tag{2}$$

where the energies are expressed in frequency units. Equation (2) is given for purposes of illustration, and an exact solution was used in reducing the experimental data to determine (E_0-E_1). The measurements were made with H near 300 G, where the field-dependent contribution was about 18 MHz. A 1-ppm precision in (E_0-E_1) represents 0.03 MHz, and hence a precision of only 1 part in 600 was required for the determination of the field-dependent term.

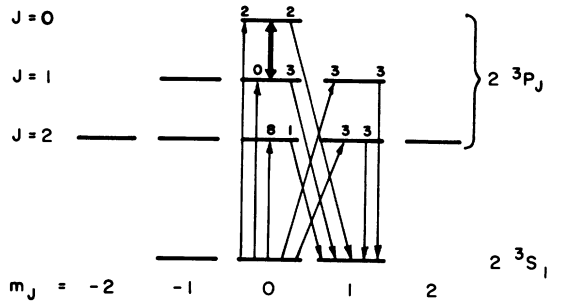

FIG. 4. Zero-field branching diagram for $2^3S \leftrightarrow 2^3P$ radiation leading to observation of $2^3S m_S=0 \rightarrow 1$ transitions. The relative intensity of the $2^3S m_S=0 \rightarrow 2^3P_{1,0}$ differs little from these values at the operating magnetic field. The double arrow indicates the microwave transition 15.

B. Signal strengths and line shapes

An expression was derived in I for the probability $P'(m_S \rightarrow m_S')$ that an atom originally in the sublevel $^3S_1(m_S)$ would transfer to $^3S_1(m_S')$ as a result of the combined effects of (a) a single process of optical excitation to and decay from the 2^3P_J levels, and (b) a microwave transition between a pair of 2^3P sublevels (α,β) with a transition probability $\rho(\alpha,\beta)$. We reproduce this expression:

$$P'(m_S \rightarrow m_S')=\frac{1}{\sum_{\mathcal{J}' m_J'}\sigma(m_S;\mathcal{J}' m_J')}\left(\sum_{\mathcal{J} m_J}\sigma(m_S;\mathcal{J} m_J)\gamma(\mathcal{J}, m_J; m_S')\right.$$
$$\left.+\rho(\alpha,\beta)[\sigma(m_S;\beta)-\sigma(m_S;\alpha)][\gamma(\alpha;m_S')-\gamma(\beta;m_S')]\right). \tag{3}$$

The symbol $\mathcal{J}$ denotes the value of J belonging to a given 2^3P level at zero-field. The optical-excitation probability from $2^3S(m_S)$ to $2^3P(\mathcal{J}, m_J)$ is denoted by $\sigma(m_S;\mathcal{J}, m_J)$, and the corresponding probability for decay from $2^3P(\mathcal{J}, m_J)$ to $2^3S(m_S')$ is represented by $\gamma(\mathcal{J}, m_J; m_S')$. These probabilities contain transformation coefficients from a (J, m_J) to a $(\mathcal{J}, m_J)$ representation, and take account of the fact that J is not a good quantum number at nonzero fields. The relative excitation and decay probabilities at zero field are depicted in Fig. 4. In the present work the 2^3P levels α, β were $(\mathcal{J}=0, m_J=0)$ and $(\mathcal{J}=1, m_J=0)$. The signal observed was the difference in final state $^3S_1(m_S'=\pm1)$ populations between microwave power on and off. The initial state was $^3S_1(m_S=0)$. The signal was normalized by dividing this difference by the population with microwave power off. We have therefore from (3) an expression for the relative signal

$$S_{m_S\rightarrow m_S'}^{\alpha\rightarrow\beta}=\frac{\rho(\alpha,\beta)[\sigma(m_S;\beta)-\sigma(m_S;\alpha)][\gamma(\alpha,m_S')-\gamma(\beta,m_S')]}{\sum_{\mathcal{J},m_J}\sigma(m_S;\mathcal{J},m_J)\gamma(\mathcal{J},m_J;m_S')} \tag{4a}$$

$$=\frac{\frac{R}{2}\rho(\alpha,\beta)\left(1\pm\frac{2\mu_B H}{(E_1-E_2)}\mp\frac{8\mu_B H}{(E_0-E_1)}\right)}{\left(\frac{13}{4}\mp\frac{2\mu_B H}{(E_1-E_2)}\right)+R\left(1\pm\frac{2\mu_B H}{(E_0-E_1)}\right)}, \tag{4b}$$

for $m_S'=\pm1$.

The second (4b), included for illustrative purposes, is correct to first order in the field H for the relevant values of α, β, m_S, m_S', and has been evaluated from the explicit engenfunctions and eigenvalues as given in I. It has been assumed that the relative intensities of the lamp for excitation to $J=0$, 1, 2 were, respectively, R, 1, 1, (see Sec. III). R was typically 0.4, and at zero field this yielded an expected relative signal of 1.9% for a microwave-field amplitude of about 2 G, [$\rho(\alpha,\beta)=0.33$, see below]. The variation of relative signal (4a) for $m_S'=\pm 1$ for our transition is shown as a function of field in Fig. 5. The microwave-transition probability $\rho(\alpha,\beta)$ was derived in I:

$$\rho(\alpha,\beta)=\frac{2(\mu_B H_1)^2|V|^2}{(\omega_{\alpha\beta}-\omega)^2+4(\mu_B H_1)^2|V|^2+\gamma^2}\ , \qquad (5)$$

where the applied microwave magnetic field has an amplitude $2H_1$ and angular frequency ω, the energy-level separation at a particular field H is $\omega_{\alpha\beta}$ and V is the time-independent part of the matrix element coupling α and β as a result of the applied microwave field. For our transition the value of $|V|^2$ at zero field is 0.667, decreasing slowly as a function of H as shown in Fig. 6. The radiative decay-rate of the $2\,^3P$ state, γ, is 1.0×10^7 sec to an accuracy of about 10%.[9] Figure 7 illustrates the variation of the signal as a function of microwave field intensity.

Equation (5) determines the lineshape of the observed signal. For very small values of H_1 the linewidth approaches the natural value (in frequency units)

$$(\Delta\nu)_0=2\gamma/2\pi\sim 3.2\ \text{MHz}.$$

Experimentally one obtains the highest statistical precision for line center determination when H_1 is such that the ratio $\rho_0(\alpha,\beta)/\Delta\nu$ is maximum, where $\rho_0(\alpha,\beta)$ is the value of $\rho(\alpha,\beta)$ at resonance, ($\omega=\omega_{\alpha\beta}$), and $\Delta\nu$ is the power-broadened linewidth. This occurs when

$$\Delta\nu=(\sqrt{3}\gamma/\pi)\sim 5\ \text{MHz} \qquad (6)$$

and

$$2H_1=\sqrt{2}\ \gamma/\mu_B|V|\sim 2G \qquad (7)$$

for transition 15. The units of μ_B are radian $\text{sec}^{-1}\ \text{G}^{-1}$. Substituting this value of $2H_1$ into Equation (5) we obtain the value $\rho_0(\alpha,\beta)=0.33$.

The above signal estimate has been made by treating the optical excitation, microwave transition, and radiative decay as separate processes. A more complete theory involving the time-dependent Schrödinger equation has been developed by Serber,[10] and this was applied in I to our experimental conditions, reducing to the same result as Eq. (4).

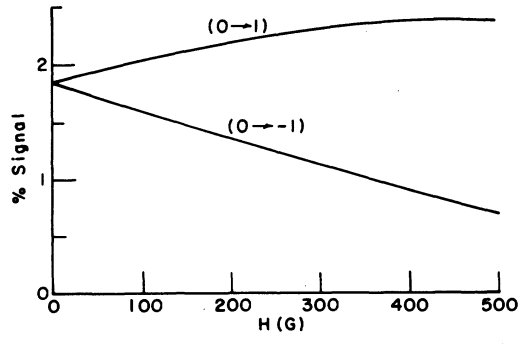

FIG. 5. Calculated signals for $0\rightarrow\pm 1$ detection schemes as a function of magnetic field.

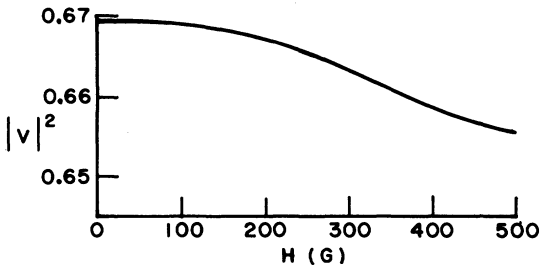

FIG. 6. Square of time-independent microwave transition matrix element between the two levels involved in transition number 15 as a function of magnetic field.

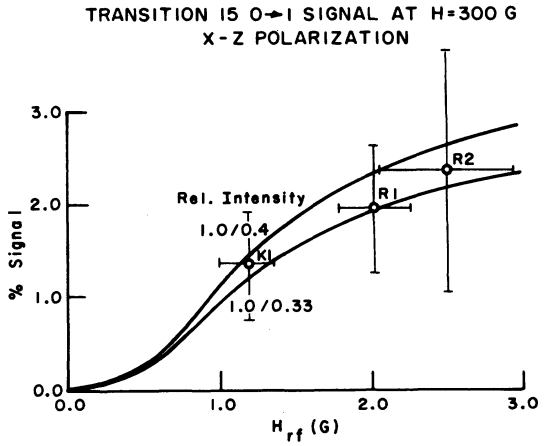

FIG. 7. Calculated signal as a function of microwave intensity at a typical value of operating magnetic field. Points are adjusted experimental signals as described in Sec. IV. The upper and lower curves are, respectively, for intensity ratios 1:0.4 and 1:0.33 for the two components of the lamp spectrum (h_2:h_1 in Fig. 11).

The experimental line shapes were obtained by sweeping the uniform field H, i.e., by varying $\omega_{\alpha\beta}$ in Eq. (5). Allowance had to be made therefore for the microwave-independent variation of signal strength with H, Eq. (4) (see Fig. 5). Detailed treatment of this correction is discussed in Sec. V, together with other factors which might have affected the line shape.

C. Choice of microwave transition

Three microwave transitions between the (0, 0) sublevel and the sublevels of the $J=1$ level can be studied to obtain the $J=0 \longleftrightarrow 1$ fine-structure separation. The signal strengths of the two $|\Delta m_J| = 1$ transitions are comparable to or smaller than the $\Delta m_J = 0$ transition. Favoring the latter is the absence of a first-order field dependence in the transition frequency [Eq. (2)] and consequently the requirement on field homogeneity is less stringent. However, the magnetic field must be varied over a wider region in order to obtain well defined resonance curves. Another factor favoring a $\Delta m_J = 0$ transition is that it allowed more convenient geometry for the design of a cavity with appropriate slits for the light and atom beams.

III. APPARATUS

The apparatus used was that described in II, with some modifications. Only those sections which were modified to meet the particular needs of this experiment will be described.

A. Electron gun

A new electron gun was designed in order to increase the 2^3S metastable beam intensity. In its final version, shown schematically in Fig. 8, the gun consisted of several thoriated tungsten filaments, 0.15 mm diameter, serving as the cathode, and a block of stainless steel as the anode. The gap between the anode and cathode was 3.18 mm. The potential difference across the gap was about 200 V. The atomic beam was close to the cathode where the electron energy was about 30 eV. Preparation and activation of the tungsten filaments followed steps which are described in the literature.[11] A factor of two improvement in metastable beam intensity was obtained with this gun as compared to that used in I, and it was estimated that the efficiency for producing 2^3S metastables was about 2×10^{-4}.

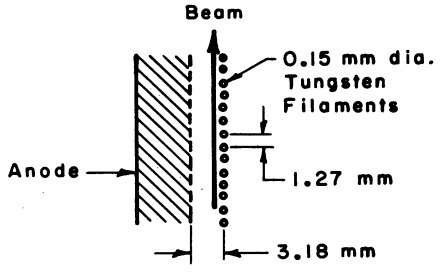

FIG. 8. Cross section of the electron gun. The magnetic field (not shown) is perpendicular to the paper.

B. Microwave system

The microwave power was generated by a two-cavity klystron[12] with a power rating of about 10 W at 29.6 GHz (Ka band). The klystron frequency was stabilized to one part in 10^7 by the scheme shown in Fig. 9. The local frequency standard was a Hewlett Packard frequency synthesizer which was periodically compared to WWVB. A 10 GHz klystron (X band) was phased-locked to this standard, and its third harmonic was mixed with the output of the Ka band klystron. The i.f. output of 400 kHz, obtained by adjusting the X-band frequency, was amplified and fed to an FM discriminator whose dc output was offset to zero at some specific frequency. Fluctuations in the Ka-band klystron output were therefore transformed to fluctuations about 0-V dc in the discriminator output. This provided a suitable error signal for electronically stabilizing the frequency.

The output of the klystron was square-wave modulated at the ferrite switch by a reference signal from the detector counting logic network

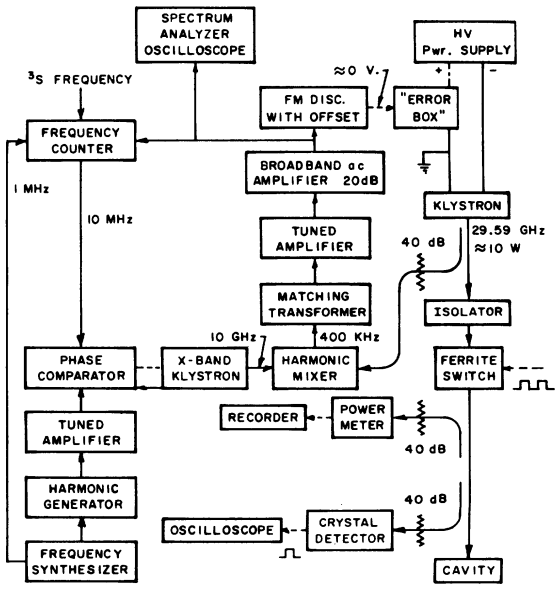

FIG. 9. Block diagram of microwave system.

(described in I). The possibility existed of using the switch as a power leveler as well, by varying the amplitude of the reference signal, but this was not attempted because monitoring the microwave power indicated that it was stable to about 1% which was as much as could be expected from the power-leveling system. Also the maximum power available was just adequate for observing an optimally power-broadened resonance line, and a power-leveling system would have necessitated a reduction in the output.

The microwave cavity, shown in cross section in Fig. 10, was constructed from a U-shaped section of R 96/U silver waveguide which was shorted at one end and iris coupled to the power source at the other. The length of the cavity (10.15 cm) was such that it sustained the $TE_{10n=14}$ mode of oscillation. A tuning screw at the shorted end of the cavity was used to keep the cavity matched to the operating frequency. Slits 0.07-cm wide were cut in the walls of the cavity for the entrance and exit of the atomic beam and for the entrance of the resonance radiation from the discharge. Both the klystron and cavity were water cooled.

C. Light source

The 10 832 Å radiation for the $2\,^3S$-$2\,^3P$ excitation was obtained from a helium rf discharge. Slight modifications to the driving circuit used in the work described in papers I and II were made. A network was inserted in the tank circuit in order to match the impedance of the load to the oscillator when the discharge was going. This reduced significantly the radiated power and made for more efficient operation of the rf oscillator. A power meter in the line monitored both the incident and reflected power.

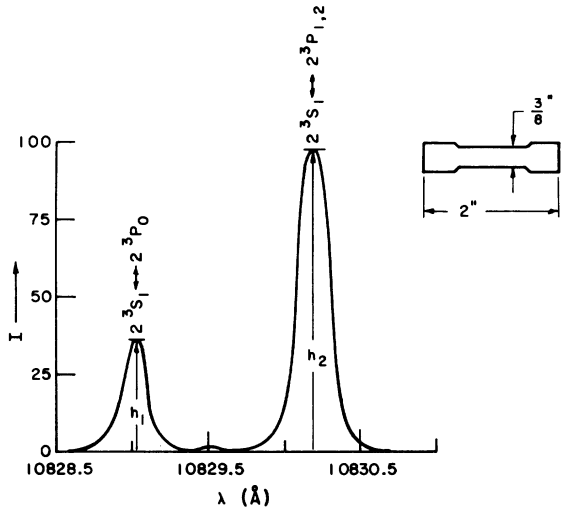

FIG. 11. A typical lamp spectrum taken with about 15 W driving power. The smaller peak h_1 alone contributes to the observed signal. Inset shows lamp dimensions.

A typical lamp spectrum is shown in Fig. 11. Many such spectra were taken as a function of the rf power driving the discharge, i.e., the incident minus the reflected power. It was observed that while both peaks increased with power, the larger peak h_2 increased at a faster rate. The larger

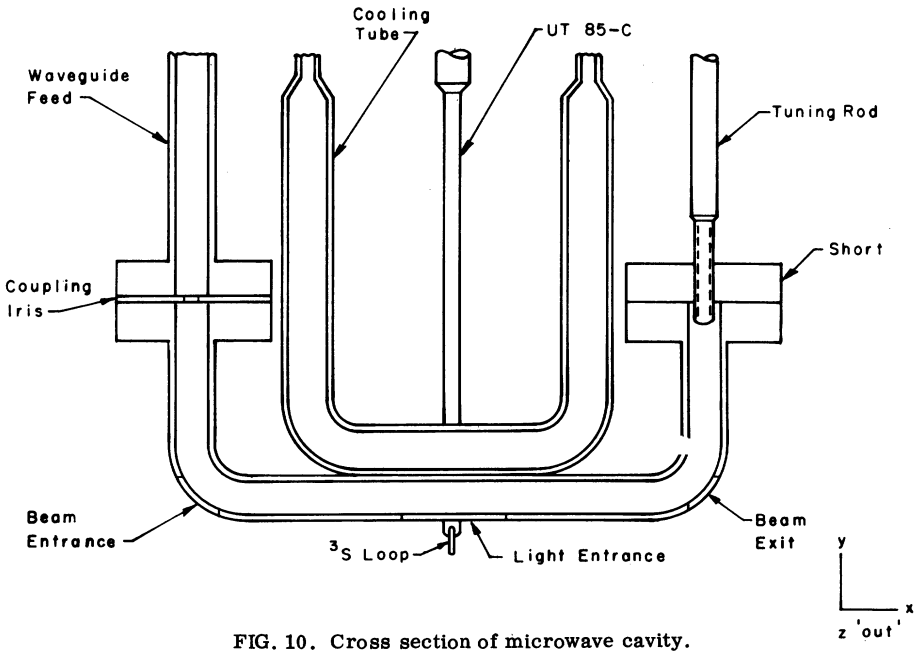

FIG. 10. Cross section of microwave cavity.

peak played a negligible role since the $2^3S(m_S=0) - 2^3P_1(m_J=0)$ excitation probability was approximately zero at our operating magnetic field (see Fig. 4). It was therefore desirable to have both h_1/h_2 and h_1 as large as possible. The operating power for a given lamp was therefore taken to be that which gave a maximum for the ratio h_1^2/h_2. Typical operating power of the discharge was 15 w.

IV. EXPERIMENTAL PROCEDURE

A. Beam studies

An earlier study[13] of the composition of a helium beam produced in a Wood's discharge tube determined the constituents to be mainly 1^1S_0, 2^3S_1, 2^1S_0 and photons, with a preponderance of the latter. We undertook a similar study for our electron bombardment source as check of the overall performance of the apparatus.

Optical excitation by a helium resonance lamp, with both deflection magnets turned off, produced an overall decrease in the beam intensity due to the processes

$$(n' \geq 2)^1S_0 \rightarrow (n \geq 2)^1P_1 \rightarrow 1^1S_0 .$$

The relevant beam profiles are illustrated in Fig. 12. It was found by inserting a filter[14] with a known attenuation of the $2^1S_0 \rightarrow 2^1P_1$ radiation, that the contributions came almost entirely from $n, n'=2$, and hence we determined that 13% of the detectable beam was due to 2^1S_0 metastables.

The 2^3S_1 population was determined using the Stern-Gerlach effect. The $m_S=\pm1$ populations were obtained directly from the difference in the profiles taken with the B magnet on and off (A magnet off), see Fig. 12(a). Corrections for the finite widths of the beam and detector and for deflections out of the range of the detector slit were made. The population of the $m_S=0$ component was set equal to the value obtained for the ±1 components. From these results it was estimated that 35% of the detectable beam was triplet metastables. The remainder of the beam, about 55%, was believed to be unidentified uv photons due to electron excitation of the beam.

The refocusing of the A and B magnets was checked. This consisted of measuring the total intensity at the detector plane of beam profiles taken with both magnets on and off, $I(4)$ and $I(5)$ in Fig. 12. The total intensity with both magnets on was 8% smaller than the intensity with both off. Since the total intensity with only B on was the same as for both A and B magnets off, the 8% decrease had its origin in the deflection at the A magnet. Also, because the deflection affects only the $m_S=\pm1$ atoms in the beam, the 8% loss in the total intensity became a larger fractional loss ($\simeq 12\%$) for these two components of the beam. This fact had to be considered in the redistribution of the $2^3S(m_S=+1)$ atoms in the beam by the optical radiation, the so-called light flop.

Under experimental conditions for observing

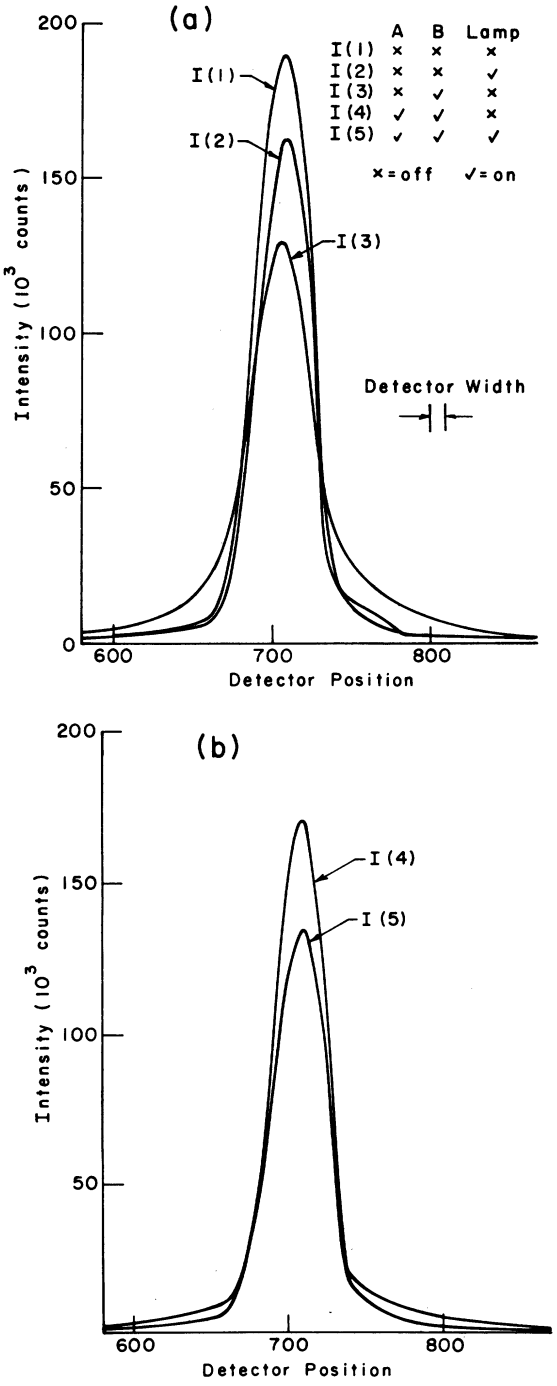

FIG. 12. Beam profiles taken with the various combinations of A, B magnets and lamp on or off defined in (a). Width of He detector slit was 0.25 mm.

the microwave resonance, the initial $m_S = +1$ and -1 components of the beam were obstructed by beam stops and therefore did not pass through the B magnet, see Fig. 2. The detector was positioned off-axis in order to observe those atoms which change their m_S value from $0 \rightarrow +1$ through optical excitation and radiative decay.

The ultimate check of the performance of the apparatus was the comparison of the calculated and observed signals. The theoretical signal has been discussed in Sec. II B. and is given by Eqs. (4) and (5). The background at the detector, arising from the tail of the undeflected beam, reduced the fractional signal. The theoretical signal must be further reduced because the signal-size calculations assume a uniform microwave field, whereas the actual field was not (Sec. V B). When these two corrections were applied to the peak observed signals, the results were in good agreement with the theoretical signals as shown in Fig. 7. The error flags are calculated from the rms errors of the fitting parameters A and B in Sec. V C.

B. Data runs

The microwave transition between the two $2\,^3P$ Zeeman levels of interest was observed by its effect on the number of atoms transferring from $2\,^3S$ $m_S = 0$ to $m_S = \pm 1$. The microwave power in the cavity was square-wave modulated on and off and the output of the detector was gated synchronously to two scalers measuring counts with microwave power on and off. The counting stopped when the counts in the off scaler reached a preset value, usually 10^6. Integration times were usually between 20 and 40 minutes.

A resonance curve was obtained by measuring the signal at several values of the magnetic field. The field values covered up to ± 100 G about the estimated line center, and points were taken in pairs at equal distances above and below the estimated center. About 20 points were adequate to give a well-defined line. Most of the points were concentrated at fields near the half-maximum signal value since these carried the most weight in determining the line center. The procedure of alternating data points above and below the line center was adopted in order to minimize the effects of slow drifts in microwave power, lamp intensity, and the magnetic field.

A small loop beneath the microwave cavity and close to the light slit was used for measuring the magnetic field (Fig. 10); the rf frequency was set to a predetermined ^3S resonance frequency, and the field varied until the $2\,^3S(m_S = 0 \rightarrow 1)$ resonance was observed in the small fraction of the beam passing through the loop. This fraction of the beam was ordinarily prevented from reaching the detector since it only diluted the $2\,^3P$ signal. Field measurements were made before and after the counting period for the $2\,^3P$ signal.

A moveable loop was used to map the magnetic field in the vicinity of the interaction region, in order to determine corrections due to field inhomogeneity and the fact that the fixed loop used in the data runs was not at the center of the interaction region. The field was found to be uniform to better than 1 in 10^4 over the entire region. Since this represents 0.1 ppm in terms of the $2\,^3P$ transition frequency, no corrections were necessary.

The last ten runs were taken with the cavity orientation reversed relative to the beam, i.e., beam entrance and beam exit were effectively interchanged in Fig. 10 in order to look for Doppler shifts (Sec. VIA).

V. DATA ANALYSIS

A. Slope correction

In the data analysis it was convenient to fit the resonance line shape to a Lorentzian in ω with three free parameters. The resonant part of the signal $\rho(\alpha, \beta)$ given in Eq. (5) is Lorentzian only if the matrix element $|V|$ is a constant. In our experiment the line shape was obtained by variation of the static magnetic field, and this involved a slight variation in $|V|$ as shown in Fig. 6. Furthermore, the nonresonant part of the signal, Eq. (4a) and Fig. 5, also varies with magnetic field because of the effect of Zeeman admixtures on the optical-matrix elements. These effects result in a systematic shift in the line center when a symmetric Lorentzian is fitted to the data. The procedure followed to correct this was first to calculate the ideal theoretical peak signal as a function of magnetic field, and then to alter the data points by fractional amounts to compensate for the variation with magnetic field. The approach differed slightly from that discussed in paper I, in that a parabolic curve, instead of a straight line, was used to get an approximate analytic expression for the calculated signal as a function of magnetic field. The parabolic fit was good to about 0.01%. The modification to the observed signal $S_E(i)$ due to this correction, called the slope correction, was $S'_E(i) = [S_E(i) - \mathrm{BASE}] \times \mathrm{Corr}(i)$, where $\mathrm{Corr}(i)$ was the fractional change in the theoretical signal. BASE was an additional parameter used in fitting some of the curves.

In the work reported in paper I, it was found necessary to increase the slope correction by

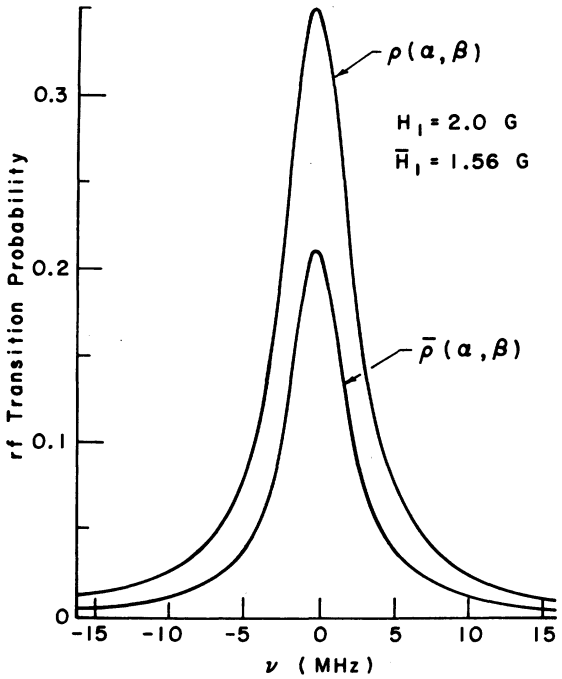

FIG. 13. Microwave-transition probabilities for uniform ρ and non-uniform $\bar{\rho}$ field distributions at the interaction region. The peak amplitude of the microwave field was 2 G.

about 25% in order to bring into agreement two sets of data taken at widely separated magnetic fields (compared to the linewidth). The probable explanation is that the experimental conditions, such as the optical polarization, differed from the conditions assumed in the signal size calculation. Since the slope correction changes ν_{01} by about 1 ppm in the present experiment, a 25% change is smaller than the statistical error. The uncertainty assigned to the correction has been taken as 25% (7 kHz). This turns out to be the largest and only significant nonstatistical uncertainty in the experiment.

B. Non-uniform microwave field

The expression for the line shape assumes a uniform oscillating magnetic field in the interaction region. If this is not the case, an averaging of the right hand side of Eq. (5) over the interaction region must be carried out. In our case the volume average simplified to a line average in the x direction because the microwave field was uniform in the y direction (Fig. 10), and the beam was very narrow compared to the dimension of the cavity in the z direction. Since the length of the interaction region was nearly equal to the guide wavelength, the effect of the averaging was significant. The variation of the microwave magnetic field along the beam (x axis) is given by $H_1\cos(2\pi x/\lambda_g)$. Therefore the space averaged Lorentzian line shape is

$$\bar{\rho}(\alpha,\beta)=\frac{1}{2\Delta x}\int_{-\Delta x/2}^{\Delta x/2}\frac{2\left(\mu_B H_1\cos\frac{2\pi x}{\lambda_g}\right)^2|V|^2}{(\omega_{\alpha\beta}-\omega)^2+4\left(\mu_B H_1\cos\frac{2\pi x}{\lambda_g}\right)^2|V|^2+\gamma^2}\,dx\,, \tag{9}$$

where Δx is the length of the interaction region. The integration was done numerically on a computer and the result is shown in Fig. 13. The transition probability ρ applies for a uniform microwave field with amplitude $2H_1$. Transition probability $\bar{\rho}$ defined in Eq. (9) is about 0.4ρ for the case shown in Fig. 13.

We note that $\bar{\rho}$ is also symmetric, but it is not a pure Lorentzian. The Lorentzian curve which fits $\bar{\rho}$ is indistinguishable from it on the scale used in the figure. In general then, one could still fit a Lorentzian to the data points to determine the line center without introducing any systematic error in the fine structure determination. However, the χ^2 of the fit and perhaps the uncertainty in determining the line center will tend to be higher. Since $\bar{\rho}$ represents an average of Lorentzians, the value of H_1 extracted from the fitted linewidth also represents some average smaller uniform microwave field over the interaction region.

C. Curve fitting

The curve-fitting procedure followed the same steps outlined in paper I. The raw data consisted of a set of values of observed 2^3P signal, each corresponding to a particular 2^3S Zeeman frequency, which was converted to a field parameter in terms of $\mu_B H$ using the value of $g_J(2^3S)$ given below.

With some assumed value of ν_{01} and the following values of the other constants,

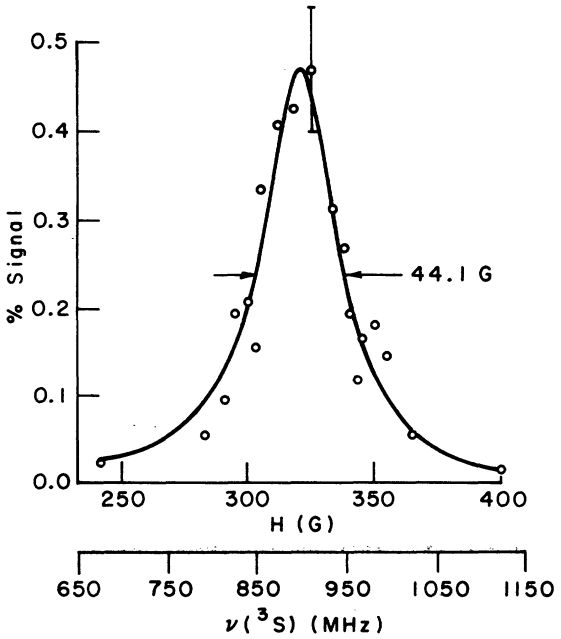

FIG. 14. Typical observed resonance line, showing percent signal versus magnetic field measured by the Zeeman transition frequency $\nu(^3S)$. The circles represent the experimental points and a typical error bar is shown. The solid curve is a Lorentzian curve fitted to the data. The klystron frequency was set at 29 596.704 MHz.

$g_J(2\,^3S) = 2.002\,237$ (Ref. 15),

$g_S - g_L(2\,^3P) = 1.002\,377$ (Ref. 1) (paper II),

$\nu_{12} = E(2\,^3P_1) - E(2\,^3P_2) = 2291.196$ MHz (Ref. 1)

(paper I as corrected in II),

values of the $2\,^3P$ transition frequencies, $\nu(^3P)$, corresponding to the field values were computed. The data were then fitted to a Lorentzian of the form

$$\text{Signal} = A/\{[\,\nu(^3P) - \nu_0]^2 + B\}\ . \qquad (10)$$

The parameters A, B, and ν_0 were determined from the fit, ν_0 being the frequency at the line center. The value of ν_0 was compared with ν_K, the klystron frequency, and the assumed value of ν_{01} was adjusted. The process was repeated iteratively until $|\,\nu_0 - \nu_K|$ was less than 1 kHz.

For the last 43 runs an additional parameter, BASE, was included in the fitting program to check for any drifts in the baseline. The magnetic field H was varied over a wider region than for the other runs so that the wings of the resonance were well defined. A typical resonance and the fitted Lorentzian are shown in Fig. 14. The four-parameter analysis was used for this curve. The full width at half maximum (FWHM) linewidth of 44.1 G corresponds to a frequency width of about 4.4 MHz. A typical error bar due to the one standard deviation statistical uncertainty is shown. Because of the small signals and large number of counts registered on the scalers, the size of the error bar for each data point was the same. Observed peak signals ranged between 0.3 and 0.8%.

The rms errors in the fitting parameters were determined from the error matrix. Errors in A and B [Eq. (10)] ranged between 20 and 60%. The error in ν_0 was taken as the error in ν_{01}. The justification for this is that a small change in ν_{01} produces an equal change in ν_0. A summary of all runs is given in Table I.

The values of ν_{01} and the rms errors were then combined to obtain a weighted mean and one standard deviation error. With the weight for the ith run defined as $W_i = 1/[\Delta\nu_{01}(i)]^2$, the weighted mean was found using the formula

$$\nu_{01} = \sum \nu_{01}(i)\, W_i \,/ \sum W_i\ .$$

The standard deviation formulas are

$$\sigma_I = 1\Big/\Big(\sum W_i\Big)^{1/2}$$

and

$$\sigma_E = \Big(\sum [\,\nu_{01}(i) - \nu_{01}]^2 W_i \,/ (N-1) \sum\ W_i\Big)^{1/2}\ ,$$

which determine, respectively, the internal and external consistency of the data. The ratio $R = (\sigma_E/\sigma_I)^2$ is equal to $\chi^2/N - 1$, where N is the number of runs used in the final analysis. The distribution of the individual results for ν_{01} about the weighted mean is illustrated in Fig. 15. The results are

$\nu_{01} = 29\,616.864$ MHz,

$\sigma_E = 0.032$ MHz,

$\sigma_I = 0.026$ MHz .

It can be seen that the value of χ^2 is somewhat larger than would be expected from purely statistical uncertainties. This probably arose from a combination of drifts during the course of a run and from the fact that the lineshape was not a simple Lorentzian. Neither of these factors should have affected the precision to which the line center was determined for the reasons discussed in Secs. IV B and V B, respectively. We have nevertheless increased the quoted uncertainty to reconcile the internal and external standard deviations.

TABLE I. Results of data analysis.

Run	Points	ν_K (MHz)	ν_{01} (MHz)	Error (MHz)	$\Delta\nu$ Width (MHz)	Base	χ^2 per degree of freedom
15*A*	17	29 594.076	29 617.701	0.409	7.786	−0	0.6
15*B*	20	29 594.076	29 617.140	0.280	6.237	−0	0.6
15*C*	14	29 594.000	29 616.571	0.631	10.334	−0	0.4
15*D*	19	29 594.000	29 617.089	0.338	6.201	−0	0.7
15*E*	21	29 594.500	29 616.344	0.488	9.644	−0	0.8
15*F*	23	29 595.380	29 617.017	0.480	10.077	−0	1.2
15*G*	16	29 595.677	29 616.375	0.539	9.028	−0	1.4
15*I*	19	29 595.578	29 616.479	0.282	6.305	−0	0.8
15*J*	20	29 595.548	29 615.967	0.343	7.483	−0	1.1
15*K*	19	29 595.590	29 617.065	0.232	5.701	−0	1.0
15*L*	17	29 595.850	29 617.380	0.301	6.474	−0	1.1
15*M*	15	29 595.780	29 615.500	0.878	14.293	−0	1.4
15*N*	9	29 595.828	29 615.895	0.651	8.937	−0	0.8
15*O*	15	29 596.415	29 617.282	0.305	5.068	−0	1.7
15*P*	17	29 596.454	29 616.611	0.258	8.693	−0	1.6
15*Q*	17	29 596.958	29 617.167	0.161	6.664	−0	1.0
15*R*	16	29 597.059	29 616.887	0.183	7.235	−0	2.5
15*S*	16	29 597.529	29 616.702	0.200	7.656	−0	1.0
15*T*	15	29 597.389	29 616.369	0.180	6.072	−0	1.5
15*V*	16	29 599.485	29 617.107	0.394	9.625	−0	1.0
15*W*	14	29 599.870	29 616.867	0.191	6.680	−0	1.9
15*X*	14	29 599.870	29 616.872	0.186	6.618	−0	2.0
15*A*1	18	29 601.146	29 616.948	0.304	6.579	−0	1.6
15*B*1	26	29 597.755	29 616.503	0.189	5.200	−0	0.9
15*C*1	22	29 598.125	29 617.007	0.348	6.208	−0	1.8
15*D*1	12	29 598.005	29 616.826	0.309	4.876	−0	0.2
15*E*1	18	29 599.335	29 616.333	0.120	3.638	−0	1.5
15*F*1	11	29 599.024	29 617.016	0.378	5.868	−0	1.7
15*G*1	10	29 600.364	29 617.371	0.271	5.293	−0	1.0
15*I*1	11	29 603.046	29 617.320	0.272	5.408	0	2.2
15*J*1	21	29 595.623	29 616.980	0.184	6.935	−0.09	0.9
15*K*1	21	29 596.146	29 616.953	0.239	3.745	0.02	0.9
15*L*1	21	29 596.148	29 616.987	0.190	4.754	0.01	0.8
15*M*1	23	29 596.184	29 616.980	0.227	6.923	−0.06	0.7
15*N*1	21	29 595.998	29 616.704	0.217	8.272	−0.14	1.3
15*O*1	18	29 596.160	29 616.726	0.203	4.192	0.04	0.8
15*P*1	20	29 596.178	29 616.857	0.225	4.183	0.01	1.7
15*Q*1	22	29 596.196	29 617.007	0.216	4.149	0.03	1.3
15*R*1	23	29 596.382	29 617.139	0.240	7.353	−0.09	1.5
15*S*1	21	29 596.460	29 617.040	0.159	3.333	0.04	1.4
15*T*1	20	29 596.433	29 616.733	0.306	8.008	−0.08	0.6
15*U*1	21	29 596.377	29 616.544	0.249	8.589	−0.17	1.5
15*V*1	21	29 596.404	29 617.159	0.285	8.743	−0.14	1.6
15*W*1	25	29 596.283	29 617.209	0.214	5.993	−0.05	1.0
15*X*1	20	29 596.823	29 616.861	0.171	5.785	−0.10	0.9
15*Y*1	22	29 596.638	29 616.817	0.266	8.657	−0.11	1.2
15*A*2	18	29 596.764	29 616.788	0.114	3.856	−0.04	0.8
15*B*2	17	29 596.584	29 616.920	0.145	3.392	0.02	0.6
15*C*2	19	29 596.704	29 616.752	0.199	4.411	0.01	0.4
15*D*2	20	29 596.803	29 616.817	0.135	3.579	−0.02	0.6
15*E*2	20	29 596.773	29 616.944	0.169	4.733	−0.05	0.7
15*F*2	20	29 597.162	29 616.968	0.171	4.599	−0.03	0.7
15*G*2	21	29 597.097	29 616.577	0.202	5.376	−0.07	0.6
15*H*2	19	29 596.940	29 616.967	0.202	3.964	0.01	1.2
15*I*2	16	29 596.310	29 617.311	0.230	5.045	−0.04	0.9
15*J*2	18	29 597.252	29 616.960	0.325	4.990	0.04	0.9
15*K*2	26	29 597.390	29 616.797	0.189	4.628	0.01	0.5
15*L*2	20	29 596.820	29 616.543	0.248	5.747	−0.05	1.8

TABLE I. (*Continued.*)

Run	Points	ν_K (MHz)	ν_{01} (MHz)	Error (MHz)	$\Delta\nu$ Width (MHz)	Base	χ^2 per degree of freedom
15*M*2	17	29 597.594	29 616.623	0.265	5.044	0.01	0.9
15*N*2	17	29 596.700	29 617.205	0.216	4.879	−0.03	0.6
15*O*2	22	29 596.700	29 616.932	0.268	6.191	0.04	1.2
15*P*2	19	29 597.810	29 616.578	0.269	6.017	0.01	1.0
15*Q*2	17	29 598.490	29 616.950	0.354	9.659	−0.12	0.9
15*R*2	15	29 598.441	29 617.437	0.305	5.587	0.05	0.5
15*T*2	24	29 599.346	29 616.921	0.250	5.660	−0.01	1.6
15*U*2	24	29 598.530	29 617.306	0.252	9.557	−0.13	0.3
15*V*2	23	29 600.264	29 617.188	0.271	5.248	0.02	0.4
15*W*2	22	29 600.300	29 616.767	0.325	6.284	0.04	0.6
15*X*2	19	29 600.660	29 616.703	0.258	5.657	0.02	0.3
15*Y*2	18	29 600.312	29 616.826	0.219	5.149	0.03	0.7
15*A*3	20	29 600.198	29 616.959	0.282	6.465	−0.02	0.3
15*B*3	9	29 600.318	29 617.019	0.158	3.751	0.02	1.7
15*C*3	26	29 600.450	29 616.656	0.198	6.432	−0.06	1.3

VI. SYSTEMATIC EXPERIMENTAL ERRORS

A. Doppler shift

The standing wave pattern in the microwave cavity could be considered as two opposite traveling waves which in the interaction region were traveling parallel and antiparallel to the atomic beam. The beam therefore saw two microwave frequencies $\nu_K \pm \bar{v}/\lambda_g$ where ν_K is the measured klystron frequency, $\bar{v}$ is a characteristic velocity of atoms in the beam, and λ_g is the guide wavelength. The observed signal was the sum of two Lorentzians equally displaced from the frequency ν_K. The center of this sum was not necessarily at ν_K however since, owing to damping in the cavity, the amplitudes of the traveling waves were not equal and the two Lorentzians were of unequal heights and widths. An estimate of the shift of the resultant line, whose shape also deviates slightly from a Lorentzian, was taken to be $\epsilon\bar{v}/\lambda_g$.

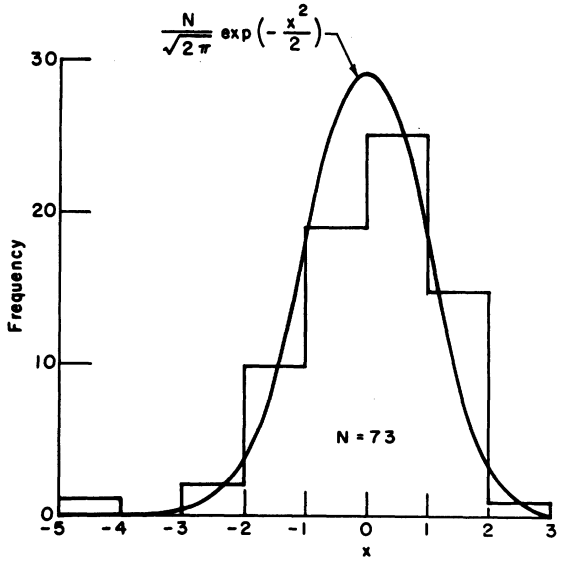

FIG. 15. Distribution of $\nu_{01}(j)$ about the weighted mean $\bar{\nu}_{01}$. The solid curve is the normalized Gaussian for $N=73$.

The quantity $\epsilon = (W_1 - W_2)/W_1$, where $W_{1(2)}$ is proportional to the square of the larger (smaller) amplitude. This factor ϵ depends on the Q of the cavity and its length. Typically, $\bar{v}/\lambda_g = 100$ kHz for a room-temperature helium beam, and for 30-GHz microwaves propagating in the TE_{10} mode in RG-96/U silver wave-guide, $\epsilon \approx 1/26$. Hence the Doppler shift is 4 kHz (0.1 ppm) in the direction of the frequency of the larger amplitude. More accurate calculations on a computer showed the shift to be even less than 0.1 ppm.

A gross experimental confirmation was obtained by taking the last 10 runs with the positions of the coupling and the short interchanged while keeping the cavity orientation unchanged. The weighted mean and one standard deviation error for this group were in general agreement with similar results of six groups of 10 runs each from the earlier runs.

B. Bloch-Siegert effect

The derivation of the Lorentzian line shape, Eq. (4), neglects the antiresonant circular rotating component of the linear oscillating field. Its inclusion results in a shift of the line center of[16]

$$\Delta\nu_0 = \frac{(\mu_B H_1/h)^2 |V|^2}{4\nu_0} ,$$

where ν_0 is the transition frequency and the other quantities have been defined in Sec. II. The shift

TABLE II. Theoretical contributions to the fine structure of 2^3P helium in MHz. The values of α^{-1}, c, R_∞, and m/M are 137.035 963 (15) (0.11 ppm), [a] 2.997 924 58 (12) $\times 10^{10}$ cm sec^{-1} (0.004 ppm), [a] 109 737.314 76 cm^{-1} (0.003 ppm), [b] and 1.370 934 $\times 10^{-4}$, [d] respectively. Thus $\frac{1}{2}\alpha^2 c R_\infty = 87.594\,31$ GHz (0.21 ppm).

Interval	$\alpha^4 mc^2$	$\alpha^5 mc^2$	$(m/M)\alpha^4 mc^2$	Second order	$\alpha^6 mc^2$	ν_{theory}	ν_{expt}	$\nu_{\text{theory}} - \nu_{\text{expt}}$
ν_{01}	29 564.587	54.708	−10.707	11.657	−3.331	29 616.914	29 616.864 [c]	0.050 = 1.69 ppm
	±0.006		±0.000 44	±0.042	±0.0039	±0.043	±0.036	
	(0.21 ppm)		(0.015 ppm)	(1.42 ppm)	(0.13 ppm)	(1.44 ppm)	(1.2 ppm)	
ν_{12}	2 317.204	−22.548	1.952	−6.866	1.542	2 291.284	2 291.196 [c]	0.088 = 38 ppm
	±0.0018		±0.000 88	±0.081	±0.0068	±0.081	±0.005	
	(0.76 ppm)		(0.39 ppm)	(35 ppm)	(3.0 ppm)	(35 ppm)	(2.2 ppm)	

[a] See Ref. 2.
[b] See Ref. 18.
[c] See Ref. 1.
[d] See Ref. 17.

$\Delta\nu_0$ is calculated to be about 40 Hz and is entirely negligible.

C. Other contributions

The possibility of contributions to the observed signal from other transitions in the 2^3P and 3^3P states was considered. The possible 2^3P transitions, $(0,0) \nleftrightarrow (1,1)$ and $(0,0) \nleftrightarrow (1,-1)$, were ruled out because they are $|\Delta M_J| = 1$ transitions, whereas the cavity was oriented to induce a $\Delta M_J = 0$ transition. Also, at the closest approach, they were still several linewidths away.

The 3^3P fine-structure splittings are roughly a factor of 8/27 smaller than the 2^3P intervals. No microwave transition in the 3^3P state would have been near enough to affect the 2^3P signal. Corrections for light shifts were not necessary as explained in Appendix B of I.

VII. RESULTS AND DISCUSSION

The sources of error which have been considered do not alter the value of ν_{01} given in Sec. VIC. σ_E is increased by 10% as mentioned in the discussion of the chi-squared, and to it is added in quadrature the estimated 7 kHz uncertainty in the slope correction. The final results are

$$\nu_{01} = 29\,616.864 \text{ MHz},$$

$$\sigma = 0.034 \text{ MHz}.$$

The uncertainty (1.1 ppm) represents one standard deviation and it is principally statistical. The value of ν_{01} is in agreement with an earlier measurement by the level-crossing technique,[6] but the quoted uncertainty is smaller by more than a factor of 10.

Table II shows the current status of the theoretical and experimental work on the 2^3P fine structure intervals. The theoretical results are broken down into the various terms of a perturbation expansion in α which was used in the calculations. The $\alpha^4 mc^2$ contribution is the Breit interaction[19] and the anomalous magnetic moment of the electron gives a correction of order $\alpha^5 mc^2$ to this term. The Breit interaction, calculated in second order and effectively summed over all intermediate configurations including the continuum, yields contributions of order $\alpha^6 mc^2$, and a recoil correction to the Breit interaction yields a term of order $(m/M)\alpha^4 mc^2$. Also at the level of $\alpha^6 mc^2$ is the lowest-order perturbation due to a spin-dependent operator of order $\alpha^6 mc^2$, first derived from the covariant two-particle Bethe-Salpeter equation by Douglas and Kroll.[20] It can be seen that theory and experi-

ment are in good agreement within their combined uncertainties.

The consistency of the ν_{01} and ν_{12} measurements can be checked by measuring the $\Delta J = 2$ transition $(0,0) \leftrightarrow (2,0)$ directly with the same apparatus. The result[21] is $\nu_{02} = 31\,908.040$ (20) MHz to be compared with the sum of ν_{01} (this paper) and ν_{12} (paper II) which is $\nu_{02} = 31\,908.060$ (36) MHz. Details of the ν_{02} measurement are given in the accompanying paper IV.

Our result for ν_{01} in conjunction with theory, can be regarded as an independent measurement of the fine-structure constant α, with the result $\alpha^{-1} = 137.036\,08 \pm 0.000\,13$ (1 ppm) compared with the more accurate currently accepted value $\alpha^{-1} = 137.035\,963 \pm 0.000\,015$ (0.11 ppm).[2]

An important level-crossing experiment in the $2\,^3P$ state has been performed recently in Paris.[22] The field values corresponding to three $\Delta m_J = 2$ crossings were measured. The authors of this work point out that their measurements cannot be used to obtain independent values of fine-structure intervals and g values. They were able to use their results, together with our values of the fine structure (paper I and this work) and our value of g'_S (paper II), to obtain a new and more accurate value of g'_L, The result is $g'_L = 0.999\,868$ (3) in excellent agreement with our earlier value (paper II) $g'_L = 0.999\,867$ (9). Both experimental values of g'_L and g'_S now differ with theory[23] by about two standard deviations.

It is of interest to compare the Paris values of the crossings with those predicted by our results for the fine-structure intervals and g'_S:

Crossing	Paris	Predicted
(J, m_J): (2, 2)-(1, 0)	562.850 (0.015) G	562.859 G
(2, 1)-(1, −1)	578.480 (0.015) G	578.489 G
(2, 2)-(0, 0)	8279.985 (0.008) G	8279.983 G

Recent experiments at Heidelberg[24] have involved measurements of the $2\,^3P$ fine-structure intervals in the two-electron ion Li^+ using dye laser saturation spectroscopy and fluorescent light detection. Unlike helium, the ordering of the $2\,^3P(J)$ levels for Li^+ is 0, 2, 1 with the $J = 0$ level lying highest. The fine-structure intervals are of the order of 100 GHz and have been measured to about 100 ppm. Theoretical calculations have not yet been done with comparable precision.

ACKNOWLEDGMENT

This research was supported in part by the National Science Foundation under Grant No. PHY 78-25655.

*Present address: Physics Department, North Carolina State University, Raleigh, N.C. 27650.
†Present address: Lawrence Berkeley Laboratory, Berkeley, California 94720.
‡Present address: Hasbrouck Laboratory, University of Massachusetts, Amherst, Mass. 01003.

[1] F. M. J. Pichanick, R. D. Swift, C. E. Johnson, and V. W. Hughes, Phys. Rev. 169, 55 (1968), referred to in the text as I. This was the first of a series of experiments on the $2\,^3P$ state of helium that have been performed by this group. The second experiment, II, was reported by S. A. Lewis, F. M. J. Pichanick, and V. W. Hughes, Phys. Rev. A 2, 86 (1970), and dealt with the Zeeman effect. Better knowledge of the Zeeman parameters improved slightly the accuracy of the $2\,^3P_1$–$2\,^3P_2$ fine structure reported in I. This paper, III, describes the third experiment which had a brief report, A. Kponou, V. W. Hughes, C. E. Johnson, S. A. Lewis, and F. M. J. Pichanick, Phys. Rev. Lett. 26, 1613 (1971). See also V. W. Hughes, in *Atomic Physics*, edited by V. W. Hughes, B. Bederson, V. W. Cohen, and F. M. J. Pichanick (Plenum, New York, 1969), p. 15; V. W. Hughes, *Facets of Physics*, edited by D. A. Bromley and V. W. Hughes (Academic, New York, 1970), p. 125.
[2] E. R. Williams and P. T. Olsen, Phys. Rev. Lett. 42, 1575 (1979).
[3] V. W. Hughes, in *Exotic Atoms '79* (Plenum, New York, 1980), p. 3.
[4] R. S. van Dyck, Jr., P. B. Schwinberg, and H. A. Dehmelt, Phys. Rev. Lett. 38, 310 (1977).
[5] I. Wieder and W. E. Lamb, Jr., Phys. Rev. 107, 125 (1957).
[6] F. D. Colegrove, P. A. Franken, R. R. Lewis, and R. H. Sands, Phys. Rev. Lett. 3, 420 (1959); J. Lifsitz and R. H. Sands, Bull. Am. Phys. Soc. 10, 1214 (1965); J. Lifsitz, Ph.D. thesis, University of Michigan, 1965 (unpublished).
[7] M. L. Lewis and P. H. Serafino, Phys. Rev. A 18, 867 (1978). This paper summarizes the operators contributing to the $2\,^3P$ fine structure and is the latest development in the theory. References to earlier theoretical work are included.
[8] W. E. Lamb, Jr., Phys. Rev. 105, 559 (1957).
[9] W. R. Bennett, Jr., P. J. Kindlmann, and G. N. Mercer, Appl. Opt. Suppl. 2, 34 (1965).
[10] R. Serber, Ann. Phys. (N.Y.) 54, 430 (1969).
[11] W. H. Kohl, *Materials and Techniques for Electron Tubes* (Reinhold, New York, 1960); M. Knoll, *Materials and Processes of Electron Devices* (Springer, Berlin, 1959).
[12] Varian Associates, Model VA-531F.
[13] V. W. Hughes, G. Tucker, E. Rhoderick, and G. Weinreich, Phys. Rev. 91, 828 (1953).
[14] Corning Type 5-57.
[15] B. E. Zundell and V. W. Hughes, Phys. Lett. 59A, 381

(1976).
[16]F. Bloch and A. Siegert, Phys. Rev. 57, 522 (1940).
[17]E. R. Cohen and B. N. Taylor, J. Phys. Chem. Ref. Data 2, 663 (1973) (for m/M_p); A. H. Wapstra and N. B. Gove, Nucl. Data A9, 267 (1971) (for $[M_p+m_e]/[M_{He}+2m_e]$.
[18]J. E. M. Goldsmith, E. W. Weber, and T. W. Hänsch, Phys. Rev. Lett. 41, 1525 (1978); B. W. Petley and K. Morris, Nature (London) 279, 142 (1979).
[19]H. A. Bethe and E. E. Salpeter, *Quantum Mechanics of One- and Two-Electron Atoms* (Springer, Berlin, 1957).
[20]M. Douglas and N. M. Kroll, Ann. Phys. (N.Y.) 82, 89 (1974); J. Daley, M. Douglas, L. Hambro, and N. M. Kroll, Phys. Rev. Lett. 29, 12 (1972).
[21]W. E. Frieze, E. A. Hinds, V. W. Hughes, and F. M. J. Pichanick, Phys. Lett. A78, 322 (1980).
[22]C. Lhuillier, J. P. Faroux, and N. Billy, J. Phys. (Paris) 37, 335 (1976).
[23]M. L. Lewis and V. W. Hughes, Phys. Rev. A 8, 2845 (1973).
[24]R. Bayer *et al.*, Z. Phys. A 292, 329 (1979).